Tensile and Fatigue Response of Steel Parts Fabricated by the Additive Friction-Stir Deposition Process

Conference Paper · February 2024

DOI: 10.1115/IMECE2023-113564

CITATION
1

READS
73

3 authors:

Chowdhury Sadid Alam
Islamic University of Technology
11 PUBLICATIONS **24** CITATIONS
SEE PROFILE

Radif Uddin Ahmed
Louisiana Tech University
11 PUBLICATIONS **13** CITATIONS
SEE PROFILE

M Shafiqur Rahman
Louisiana Tech University
33 PUBLICATIONS **121** CITATIONS
SEE PROFILE

Proceedings of the ASME 2023
International Mechanical Engineering Congress and Exposition
IMECE2023
October 29-November 2, 2023, New Orleans, Louisiana

IMECE2023-113564

TENSILE AND FATIGUE RESPONSE OF STEEL PARTS FABRICATED BY THE ADDITIVE FRICTION-STIR DEPOSITION PROCESS

Chowdhury Sadid Alam, Radif Uddin Ahmed, and M Shafiqur Rahman
Department of Mechanical Engineering,
Louisiana Tech University,
Ruston, LA, USA

ABSTRACT

Additive Friction Stir Deposition (AFSD) is a relatively new solid-state additive manufacturing (AM) process that utilizes frictional heating and plastic deformation for the layer-by-layer deposition of materials (e.g., metals and alloys). This study characterizes the mechanical behavior of AFSD-processed AISI 4340 steel parts under various tensile and fatigue loading conditions. A distinct scale of AISI 4340 steel specimens, namely the standard ASTM rectangular dog bone specimen is considered for the analysis. A finite element (FE) model is developed to predict the tensile and fatigue behavior of AFSD-processed steel AISI 4340 parts under multiple loading circumstances. The FE model can generate results for the von-Mises stress, strain, total deformation, fatigue life, factor of safety, and fatigue limit under various loading conditions. Experimental data for the tensile and fatigue responses are compared with the mechanical behavior obtained from the FE model at room temperature. The modeling results for the maximum tensile stress, deformation, and fatigue life exhibit excellent agreement with the experimental findings, which successfully confirms the validation of the FE model. The FE modeling for the fatigue analyses is conducted for a unit load ratio and by applying zero-based cyclic loads at different frequencies. Results from the current study successfully lead to generating a stress-life curve for the AFSD-processed AISI 4340 steel parts. According to the findings, the AFSD-processed components show higher strength than that of the parts created by conventional manufacturing techniques. In all cases, the AFSD specimens show extended lifespan compared to the conventionally manufactured specimens.

Keywords: Tensile properties, fatigue, AISI 4340, finite element, Additive Friction Stir Deposition.

NOMENCLATURE

E	modulus of elasticity
σ	flow Stress
ε	equivalent plastic strain
T^*	homogenous temperature
N_f	number of cycles/fatigue life
n	safety factor
S	stress

1. INTRODUCTION

Additive Friction Stir Deposition (AFSD) is an emerging solid-state additive manufacturing (AM) process for fabricating three-dimensional (3D) fully dense metallic structures that has led to significant improvements over the conventional AM techniques. In AFSD, a hollow rotating tool travels and deposits material on top of a substrate while maintaining frictional contact among the tool-material-substrate interfaces. Heat is generated due to the friction which eventually deforms the material plastically during deposition, keeping it below the melting point. This allows equiaxed fine microstructures and wrought-like mechanical properties with minimal defects. By far the only metal additive manufacturing process capable of producing wrought or comparable mechanical characteristics in the as-printed state is AFSD [1, 2]. As the forging counterpart of fusion-based additive 3D manufacturing processes, AFSD has enormous potential in the aerospace, automotive, and defense industries and deserves special attention. However, the quality of the AFSD-processed parts depends largely on the correct combination of the process parameters and understanding the complex mechanism of the material flow and temperature distribution in the deposited layers.

The AFSD process significantly improves the microstructural grains in metals and alloys as observed from recent studies. Joshi et al. [3] deposited AZ31B-Mg alloy (Mg: 97 %, Al: 2.5–3.5 %, Zn: 0.60–1.40 %, Mn: 0.20 %, Si: 0.10 %, Cu: 0.050 %, Ca: 0.040 %, Fe: 0.005 %, and Ni: 0.005 %) using AFSD technique. The microstructure of the deposition showed stronger equiaxed grain structures. The Vickers hardness of the

Contact author: srahman@latech.edu

AFSD deposited sample was also found to be stronger than its regular feed material. Beladi et al. [4] performed an AFSD deposition of SS316L steel and it was found to have extremely fine equiaxed grain structures. Perry et al. [5] explored an AFSD-process using AA 2024 as a tracer-based feed material on top of an aluminum 6061 alloy (AA 6061) substrate, where the material grain size rapidly decreased from 25–30 μm to 1–2 μm. The authors established a quantitative relationship between the strain and tracer grain size from their detailed microstructural study. Chen et al. [6] investigated the influence of AFSD process parameters (rotational speed and feed rate) on the mechanical properties and microstructure of AA 6061. Ultimate tensile strength and elongation at break was found to have a positive correlation with tool rotational speed and material feed rate. Martin et al. [7] evaluated the properties of AFSD repair of cast aluminum Mic 6 alloy using AA 6061-T6 as a filler material. The hardness of the filler alloy reached equivalence to the naturally aged T4 condition (i.e., solution heat treated and naturally aged to a substantially stable condition). It was also observed during tensile testing that under appropriate processing conditions the strength of deposited AA 6061 could match the strength of Mic 6 substrate. A study was performed by Mason et al. [8] where stacking of one layer of AA 7050 was executed perpendicular to the next one using AFSD. They conducted both microstructural and mechanical property analysis of the AFSD-processed AA 7050. Tensile testing was carried out in three different locations to measure the yield strength and ultimate tensile strength. In another investigation, AFSD of die cast A356 alloy was performed by Alzahrani et al. [9] under constant speed and different material feed rates. They conducted a microstructural and mechanical analysis, where a significant grain structural improvement and higher hardness value were achieved for all the feed rates.

A finite element model for the analysis of mechanical properties of AFSD-processed parts can lead to rapid and cost-effective alternatives before implementing the AFSD process on practical applications. Rahman et al. [10, 11] performed similar research on developing FE model for tensile and fatigue behavior of laser powder-bed fused Ti-6Al-4V specimens at room [10] and high temperature applications [11]. They showed that an experimentally validated FE model could generate reliable results for the mechanical response of AM specimens. However, at the current state of the art, there is little information on the AFSD-processed 4340 steel parts and their mechanical properties. The 4340 steel has numerous applications in automotive, aerospace, oil and gas industries, machinery, construction, transfer systems, and manufacturing industries.

In this study, the tensile and fatigue behavior of the AFSD-processed fully dense AISI 4340 specimens are characterized by developing explicit dynamics and static structural FE models. The FE simulations are conducted in ANSYS 2022 R2 to obtain results for von-Mises stress, ultimate tensile stress, strain, deformation, fatigue life, and safety factor under various operating conditions. Results obtained from simulation are validated by comparing them with the experimental results. The overall study indicates that a robust computational analysis of the mechanical properties of the AFSD-processed materials leads to reliable, low-cost, and high-efficient engineering components at various conditions.

2. MATERIAL AND METHODS

The material considered for this analysis is an AFSD-processed 4340 steel alloy containing chromium, molybdenum, nickel, carbon, manganese, sulphur, and silicon. It is known for its high strength and being widely used in aerospace, defense, automotive, and manufacturing industries. Selecting and assigning the appropriate material properties during the analysis is very critical to implementing a well-posed FE model. The material properties depend on the chemical composition and the type of processing the material. Table 1 shows the chemical composition of 4340 steel alloy as a mass percentage.

TABLE 1: CHEMICAL COMPOSITION OF AISI 4340 STEEL ALLOY AS MASS PERCENTAGE [12]

C	Mn	P	S	Si	Cr	Mo	Ni	Fe
0.43	0.71	0.01	0.02	0.23	0.73	0.24	1.65	Bal.

The mechanical properties of the 4340 steel considered in these explicit dynamics simulation are density, specific heat, bulk modulus, shear modulus, and the Johnson-Cook strength properties including yield stress, hardening constant, melting temperature, strain rate constant, and thermal softening exponent [13]. As these properties vary with temperature, it is important to incorporate the properties correctly in the FE model [14]. Table 2 shows the material properties of 4340 steel used in the model for the tensile test simulation and validation at room temperature (22°C) [13].

TABLE 2: MATERIAL PROPERTIES OF 4340 STEEL FOR EXPLICIT ANALYSIS [13]

Properties	Value
Specific Heat	477 J/kg°C
Bulk Modulus	159 GPa
Initial Yield Stress	792 MPa
Hardening Constant	510 MPa
Hardening Exponent	0.26
Strain Rate Constant	0.014
Thermal Softening Exponent	1.03
Melting Temperature	1519.9°C
Shear Modulus	81,800 MPa

The specimen selected for this study is an ASTM E8M subsize flat AFSD-processed 4340 steel dog bone structure with a rectangular cross-section [10]. The dimensions of the specimen (in mm) are shown in Fig. 1.

The proposed FE model can predict the material behavior under high strain rates and temperatures. The model relates the flow stress of the material with the temperature, strain rate and other related parameters.

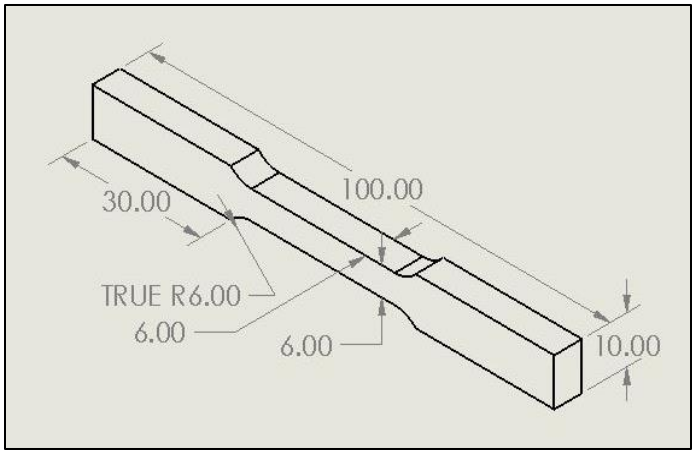

FIGURE 1: THE SUB-SIZE E8M FLAT DOGBONE SPECIMEN WHERE THE DIMENSIONS ARE IN mm [10]

AFSD process simulations can be done using Johnson-Cook Plasticity model [14], a widely used empirical model for FE analysis, that gives the stress formulation as in Eq. (1).

$$\sigma = (A + B\varepsilon^{n})(a + Cln\varepsilon^{*})(1 - T^{*m}) \quad (1)$$

Here, σ is the flow stress, ε is the equivalent plastic strain, ε^{*} is the dimensionless plastic strain rate, $T^{*}$is the homogenous temperature, and A, B, C, and m are material constants [14].

For the tensile tests of the AFSD-processed parts, Johnson-Cook strength properties for steel alloy are used as inputs in the FE model to find out the stress-strain and fatigue responses. The ASTM E8M dog bone structures are cut from a large block of 4340 steel alloy manufactured by AFSD process in a MELD machine. This cutting process is necessary because the deposition thickness and width in the MELD machine are bigger than the size of a dog bone structure. The block is initially printed in horizontal build orientation, i.e., the printing direction is perpendicular to the layering direction on a flat pane. This configuration makes the specimen stronger for the tensile tests as the tension load is parallel to the layers. Therefore, the analysis and results represented in this study are based on the horizontally printed parts.

3. THE FINITE ELEMENT MODEL

In this study, a 3-D CAD model is created in SolidWorks 2020 and imported in ANSYS Workbench 2022 R2 for the FE modeling. The physical and computational domain with the initial and boundary conditions are discussed in this section.

3.1 Physical and Computational Domain

Figure 2 shows the configuration of the physical domain, which consists of a solid AFSD-processed 4340 steel dog bone structure having a rectangular cross-section. One side of the specimen is fixed, and the other side is subjected to displacement toward positive *x*-direction due to tensile force.

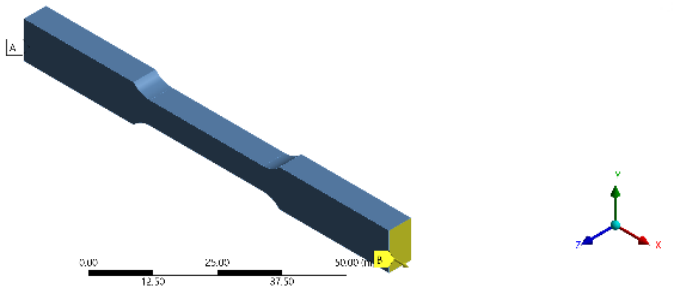

FIGURE 2: PHYSICAL DOMAIN OF THE ASTM E8M SUBSIZE FLAT DOGBONE MODEL

Figure 3 shows the 3-D mesh of the computational domain for the ASTM E8M sub-size flat model, where 186,900 rectangular elements are connected by their nodes. This is the converged mesh size which is used for the entire analysis. The mesh convergence study for the model is conducted targeting the mesh sensitivity with respect to the von-Mises stress at the room temperature.

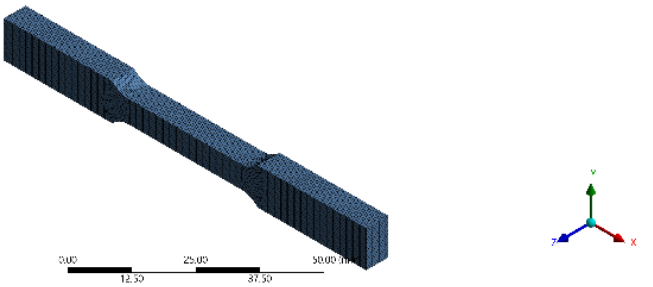

FIGURE 3: COMPUTATIONAL MESH WITH 186,900 ELEMENTS

The result of the mesh convergence study for the modeling of the flat dog bone specimen is shown in Fig. 4. The maximum von-Mises stress value in the area-transition location (at the top surface) is targeted for the mesh convergence study of the dog bone specimen model. As the number of elements increases, the maximum von-Mises stress corresponds to the tensile load to a converged mesh assembly of 186,900 elements. The mesh convergence study is conducted for the explicit dynamics FE modeling at 22°C temperature. Afterwards, static structural modeling was done for obtaining the fatigue test results with the same specimen.

3.2 Boundary and Initial Conditions

The initial temperature of the specimen is set at room temperature, i.e., 22 °C in the simulation. The film coefficient value on the surfaces of the specimen is set as 10^{7} W/m^{2}K. The boundary and loading conditions applied in the static structural simulation are shown in Fig. 2. Force applied axially in the positive *x*-direction at one side causes the displacement and the other side is kept fixed. Force is increasingly applied in the same direction until the material fails.

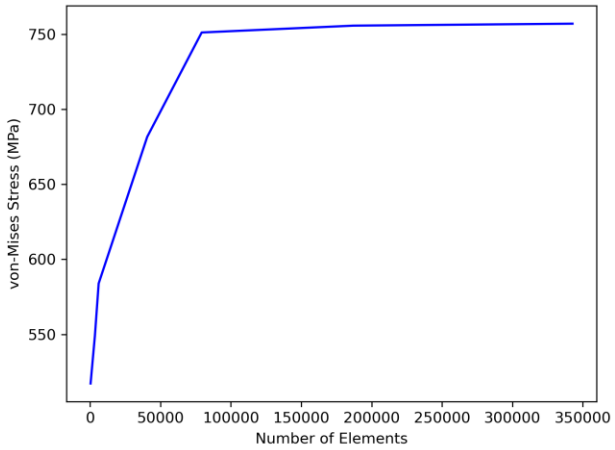

FIGURE 4: MESH SENSITIVITY STUDY FOR THE FINITE ELEMENT SIMULATION

The fatigue analysis requires alternating stress data for the 4340 steel specimens. Due to the unavailability of the data for AFSD-processed 4340 steels, WIP-C1 (Ni/CrC) coated 4340 steel processed by cold spray technique is considered in the fatigue simulation. The stress-life data for 4340 steels coated with WIP-C1 (Ni/CrC) is shown in Table 3 [15].

TABLE 3: ALTERNATING STRESS DATA FOR THE 4340 STEEL COATED WITH WIP-C1 (Ni/CrC) [15]

Cycles	Alternating Stress (MPa)
3794	637
15726	530
26688	495
59291	424
1091986	389
1.1905×10^5	371
2.9111×10^5	352

The constant-amplitude zero based cyclic load is applied at 50 Hz in the HCF tests. The schematic of the cyclic load input considered for this study is shown in Fig. 5.

4. SIMULATION PROCEDURE

The FE simulations are performed in ANSYS Workbench 2022 R2 using explicit dynamics and static structural simulations to find out the tensile and fatigue properties respectively. The temperature-dependent material and mechanical properties of AFSD-processed 4340 steel alloy are assigned in the Engineering Data before importing the geometry and meshing. Material properties are set up in the Engineering Data input during the simulation in ANSYS. The tension test simulation is conducted first to find the stress and strain data from the specimen. For the tensile and fatigue analyses, the axial loads (cyclic) are varied from low to high magnitudes (zero based) to generate results for the total deformation, fatigue life, damage, and safety factor of the FE model. The model uses Goodman criterion while analyzing the fatigue limits using stress-life method (Fig. 5).

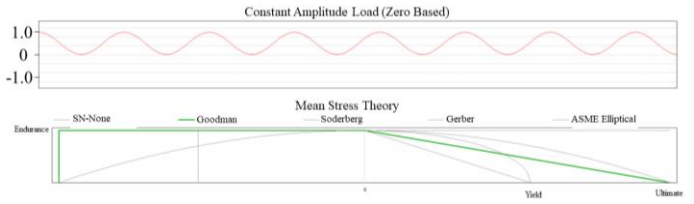

FIGURE 5: CONSTANT AMPLITUDE CYCLIC LOAD AND SOLUTION CRITERION

5. MODEL VALIDATION

The simulation results for tensile stress at room temperature are compared with the experimental results carried with 4340 steel alloy followed by performing fatigue tests applying a unit scale ratio and a sinusoidal frequency of 50 Hz at 22°C and relative humidity of 45% for base 4340 steel alloy. Fatigue tests for the tension-tension cycles were stopped when the dog bone specimens broke, or the fatigue cycles reached an order of 10^5 cycles. The FE results for ultimate tensile strength of the AISI 4340 steel specimen cold sprayed at room temperature are compared with the experimental results (Fig. 6).

The comparison is shown in Table 4 as the FE model predicts the ultimate tensile strength maintaining a good agreement with the experimental data obtained for the 4340 steel alloy.

TABLE 4: COMPARISON OF THE MODELING RESULTS WITH THE EXPERIMENTAL RESULTS

Parameters	Experimental result	Simulation result	Deviation (%)
Tensile Yield Strength (MPa)	795	792	0.37
Ultimate Tensile Strength (MPa)	890	883.03	0.78
Endurance Limit (MPa)	353	330.45	6.38

For predicting the fatigue life of the AFSD-processed specimen, a 4340 steel base specimen coated with WIP-C1 (Ni/CrC) by cold spray is considered. Due to the lack of stress-life data and associated explicit properties of the AFSD-processed 4340 steels, the authors used the fatigue properties of the cold spray coated specimens only for the model validation [15]. Cold spray is another solid-state additive manufacturing technique where the mechanical properties of the parts are comparable with the AFSD-processed parts. In cold spray technique, spray particles undergo significant plastic deformation upon impact while still solid and at temperatures maintained below their melting points [16]. All other analyses are conducted considering the fully dense AFSD-processed 4340

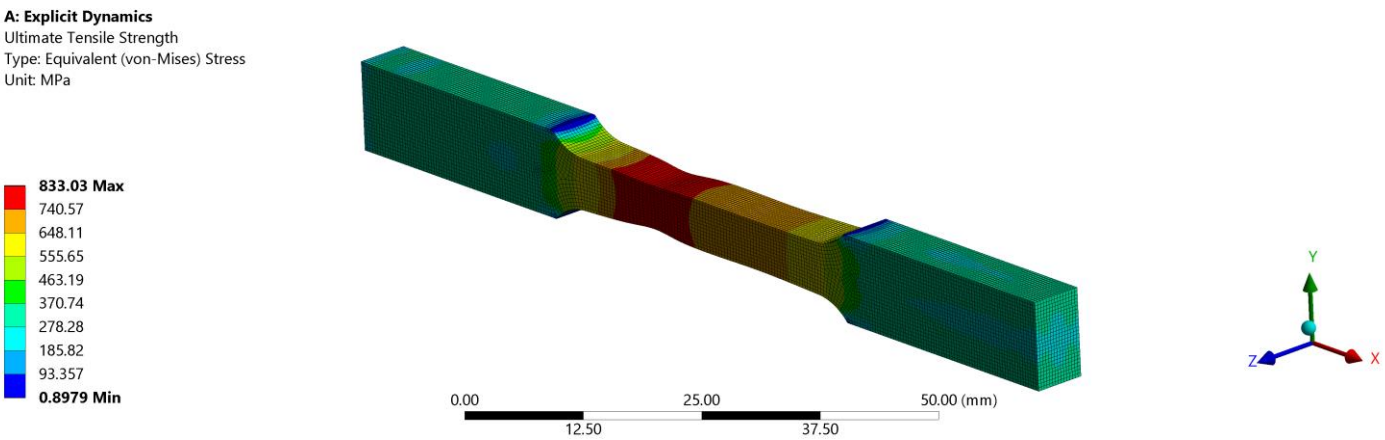

FIGURE 6: TENSILE TEST FOR MODEL VALIDATION (UTS)

steel parts. The tensile specimens are made with tool rotation speed of 800 rpm, tool traverse speed of 4.23 mm/s, and a material deposition rate of 0.42 mm/s. The AFSD process refines the microstructure grains and leads to improvement of certain mechanical properties due to equiaxed fine microstructure.

6. RESULTS AND DISCUSSION

The mechanical properties of metal alloy are widely influenced by its microstructure. The microstructure grain size, shape, and orientation are the main factors in the determination of mechanical responses. A smaller grain size in metal alloys generally lead to a higher strength and hardness. The smaller sized grains restrict the movements of dislocation, which makes grain propagation harder and leads to enhanced mechanical properties. Moreover, equiaxed grains having similar dimensions in all direction give better isotropic mechanical properties compared to other grain shapes. Alloys containing a second-phase particle or precipitate dispersed in the microstructure. They can act as obstacles to dislocation movement in the microstructure grain and improve the strength and hardness of the material. As a solid-state metal additive manufacturing process, allows for a significant strain hardening in the plastic zone of the material. The process results in small and equiaxed microstructure grains in the additive friction-stir deposited parts which ultimately leads to improving the mechanical properties, e.g., tensile, fatigue life, and hardness. The FE model presented in this study incorporates the improved properties of the AFSD-processed material and generates outputs for tensile and fatigue responses at various loading conditions.

6.1 Tensile Properties

The room temperature specimen is taken to the explicit dynamics module to apply tensile load and run tensile tests. The FE results show that the tensile and fatigue strengths of AFSD processes 4340 steel alloy decrease with the increase of loads. Therefore, the specimen is more likely to fail during the applications of tensile and fatigue loads due to added stress and deformation. The contour plots for the von-Mises stress show the specimen in yield point and ultimate strength point in Fig. 7 and Fig. 8 respectively, where the stress is shown in MPa. The yield point and ultimate strength point of the AFSD-processed parts are significantly higher than the conventionally manufactured 4340 steel alloy with values of 1063.70 MPa and 1232.30 MPa respectively.

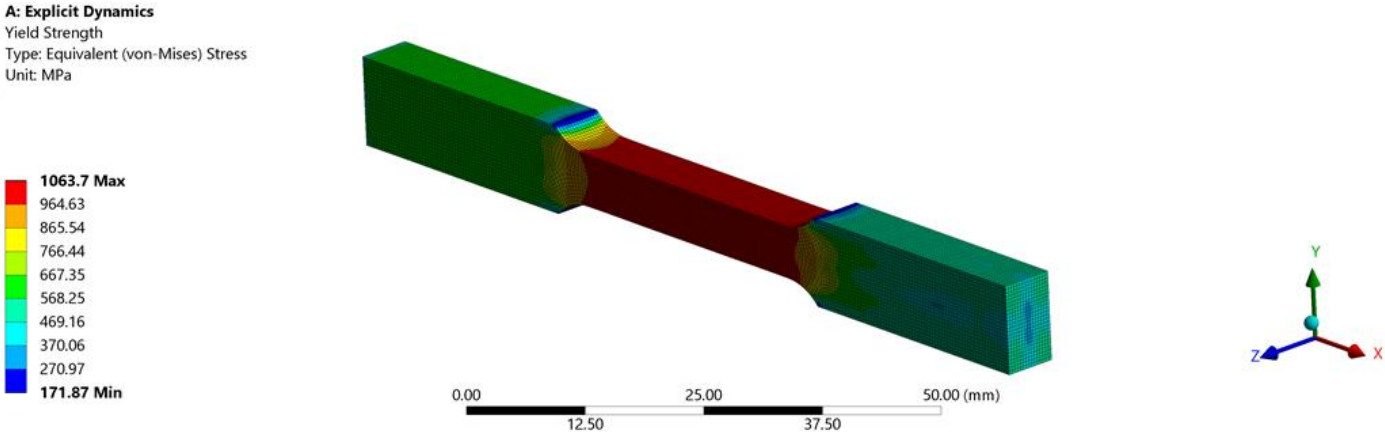

FIGURE 7: VON-MISES STRESS CONTOUR DURING THE TENSILE EXPERIMENT AT YIELD POINT

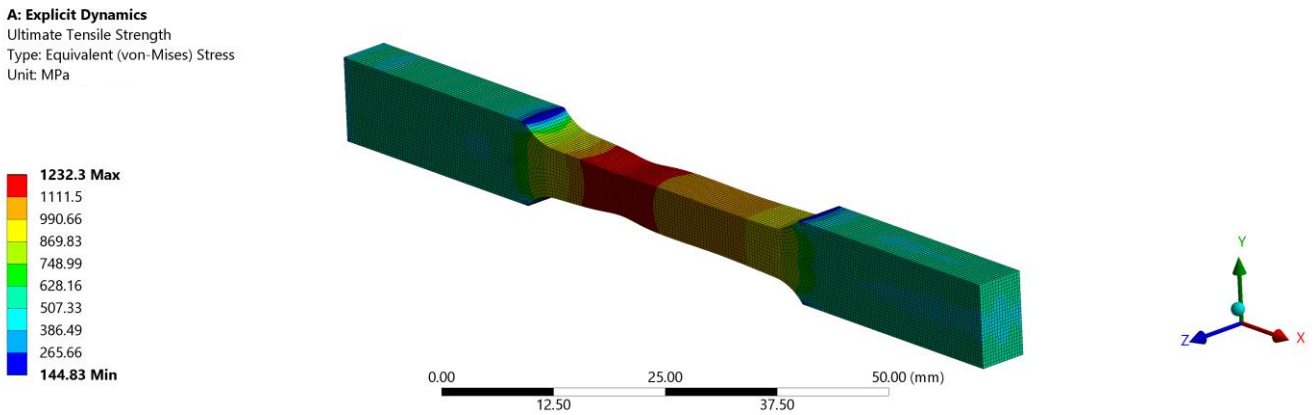

FIGURE 8: VON-MISES STRESS CONTOUR DURING THE TENSILE EXPERIMENT AT ULTIMATE TENSILE STRENGTH POINT

The neck formation during the tensile test of the specimen (Fig. 8) occurs close to the fixed end inside the narrow region. The dog bone model has a change in the cross-sectional area from both sides. Due to the cross-sectional area reduction from the fixed area to the gauge area, the stress concentration becomes high in the region close to the area change zone from the fixed end. This phenomenon leads the dog bone specimen to fail or form necking toward the fixed end rather occurring at the middle of the specimen.

As expected, the von-Mises stress and deformation increase as the magnitude of the tensile load increases. The FE simulations are conducted using the simulated physical properties of AFSD processes material fabricated in the MELD L3 Machine. Figure 9 shows the stress-strain plot achieved for the AFSD parts and compares it with the one achieved from the tests with annealed 4340 steel alloy [17]. The Johnson-Cook plasticity model is used for the stress-strain behavior above the yield point [14]. It is evident AFSD-processed 4340 steel samples withstand higher tensile strength and better plastic properties compared to annealed 4340 steel samples (Fig. 9) [17].

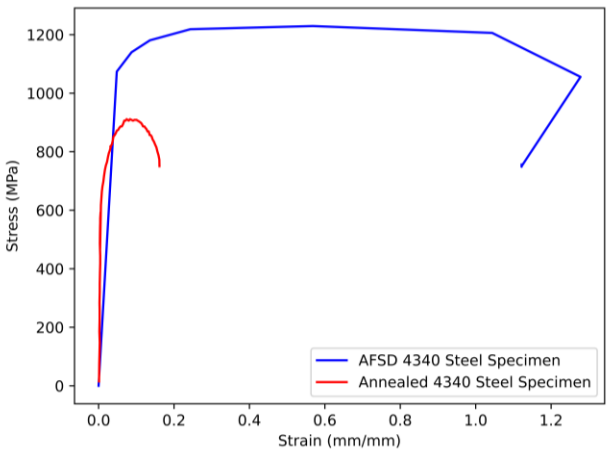

FIGURE 9: STRESS-STRAIN CURVE FOR THE AFSD-PROCESSED 4340 STEEL SPECIMEN

The force reaction vs the displacement (total deformation) curve during the tensile test is shown in Fig. 10.

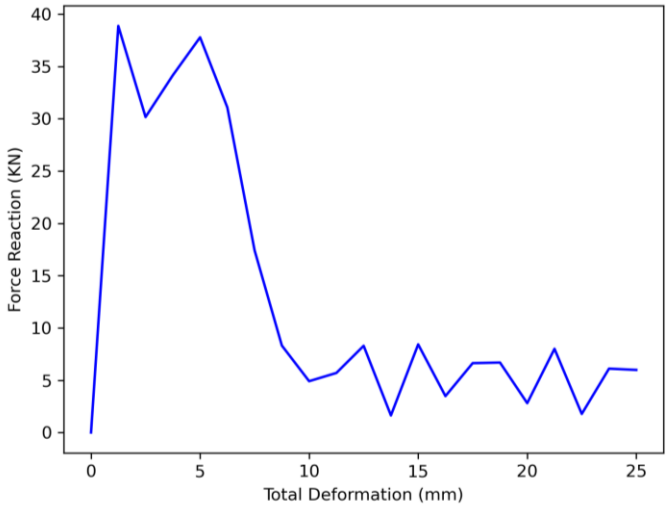

FIGURE 10: FORCE REACTION VS DISPLACEMENT FOR AFSD-PROCESSED SPECIMEN

6.2 Fatigue Properties

The ASTM dog bone specimen is analyzed in the static structural module for high cycle fatigue test applying a unit scale ratio and a sinusoidal frequency of 50 Hz at 22°C and relative humidity of 45% for base 4340 steel alloy. Results for the fatigue life of the AFSD-processed 4340 steel specimens are obtained keeping the stress ratio s kept to a unity and high-stress amplitudes were obtained as sustained by the material without fracture.

Figure 11 shows the predictions of life-cycle, safety factor and equivalent alternating stress contours for the case of 20 kN alternating tensile force at the free end of the specimen. The fatigue failure is again likely to happen at the area transition zone as seen in the contour plots.

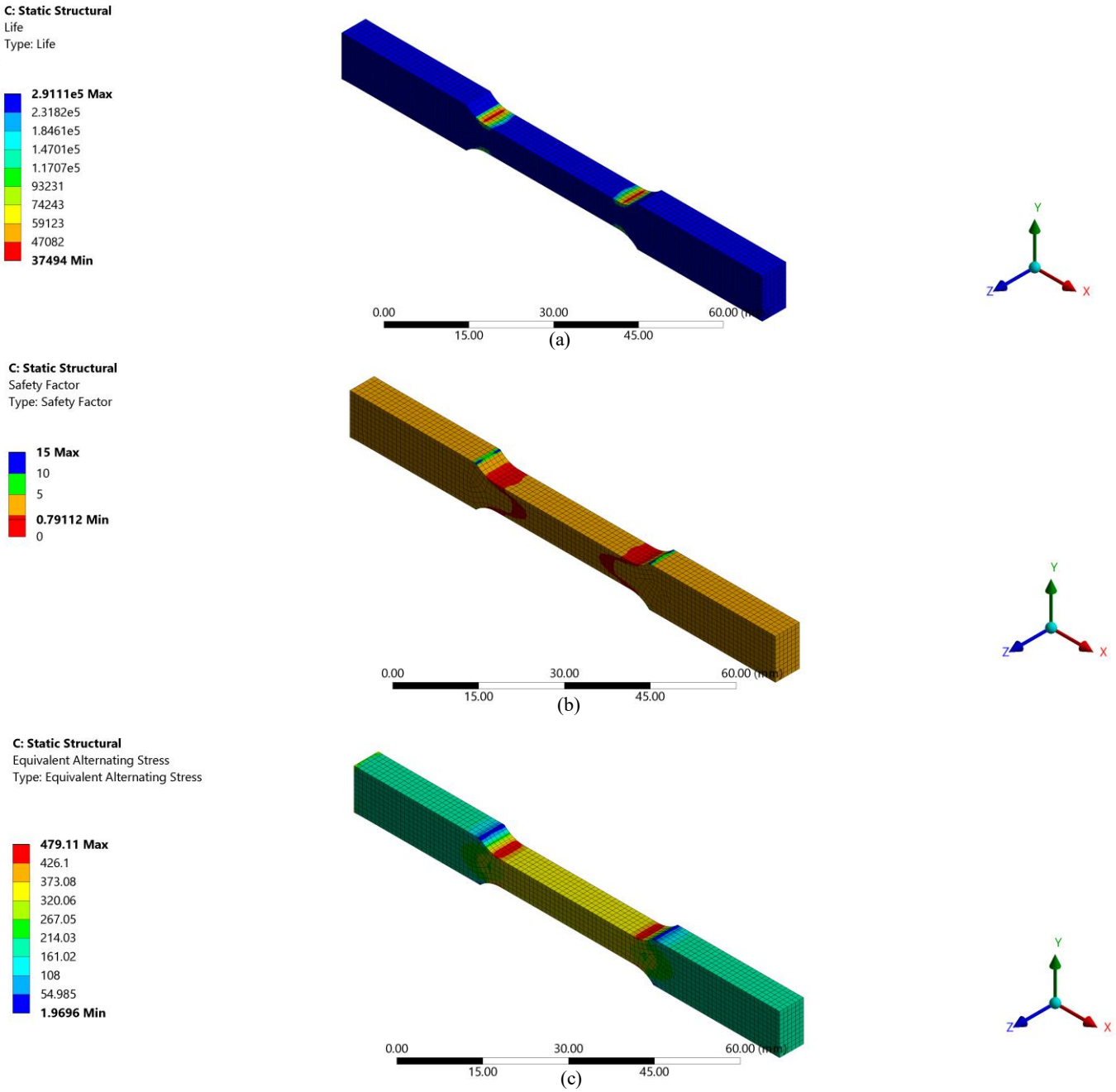

FIGURE 11: CONTOUR PLOTS FOR (a) LIFE CYCLE, (b) SAFETY FACTOR, AND (c) EQUIVALENT ALTERNATING STRESS AT A FATIGUE LOAD OF 20 kN

Figure 12 shows the stress-life diagrams obtained from the FE model where the number of cycles is plotted against the values of the alternating stress the specimen can sustain when it is subjected to axial fatigue load. Following the Goodman theory, the applied cyclic loads varied from lower to higher magnitudes until the fatigue life reaches almost zero value. From Fig. 12, the AFSD-processed materials sustain for more life cycles compared to the conventionally manufactured alloy.

The safety factor for different fatigue loads is plotted and shown in Fig. 13. The values of safety factor decrease as the magnitude of the applied load increases. The factor of safety for the AFSD-processed specimen under the same magnitude of the load is much higher than that of the conventionally manufactured specimen. The values of safety factor decrease as the magnitude of the applied load increases. The factor of safety for the conventionally manufactured specimens shows a lower value under the same magnitude of force when compared to that of the

AFSD-processed specimens. For instance, safety factor of the conventionally manufactured steel specimen at 15 kN fatigue load shows a value of 0.97 whereas the AFSD-processed 4340 steel specimens under the same fatigue load gives a safety factor of 1.13.

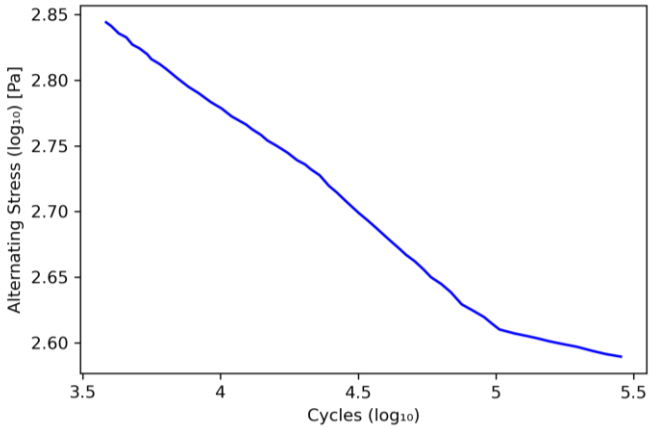

FIGURE 12: STRESS–LIFE CURVE SHOWING THE FATIGUE BEHAVIOR OF THE 4340 STEEL SPECIMEN AT ROOM TEMPERATURE

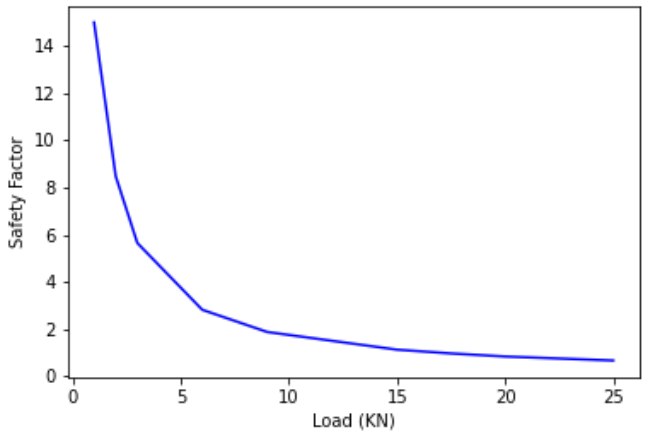

FIGURE 13: FATIGUE SAFETY FACTORS AT VARIOUS APPLIED LOADS FOR AFSD-PROCESSED 4340 ALLOY

7. CONCLUSION

A combined explicit dynamics-static structural 3-D finite element model is developed to predict tensile and fatigue behavior of a steel alloy manufactured by the additive friction stir deposition (AFSD) process. Results for tensile strength, elongation, and fatigue life of the AFSD-processed 4340 steel parts provide a detailed understanding of the metallurgical and mechanical properties of this alloy. AFSD-processed parts have higher strength and fatigue life than that of the conventionally manufactured alloys. The finite element model presented provides a faster yet reliable solution than costly experimentations. The overall study also provides a guide to investigate the mechanical properties of other high entropy materials that can be used in the AFSD process.

ACKNOWLEDGMENT

This work is supported by the U.S. National Science Foundation under grant number OIA-1946231 and the Louisiana Board of Regents for the Louisiana Materials Design Alliance (LAMDA).

REFERENCES

[1] Tuncer, N. and Bose, A., 2020, "Solid-state metal additive manufacturing: A Review," JOM, **72**(9), pp. 3090–3111.

[2] Rivera, O. G., Allison, P. G., Jordon, J. B., Rodriguez, O. L., Brewer, L. N., McClelland, Z., Whittington, W. R., Francis, D., Su, J., Martens, R. L., and Hardwick, N., 2017, "Microstructures and mechanical behavior of Inconel 625 fabricated by solid-state additive manufacturing," Materials Science and Engineering: A, **694**, pp. 1–9.

[3] Joshi, S. S., Patil, S. M., Mazumder, S., Sharma, S., Riley, D. P., Dowden, S., Mishra, R. S., and Dahotre, N. B., 2022, "Additive Friction Stir Deposition of AZ31B Magnesium Alloy," Journal of Magnesium and Alloys, **10**(9), pp. 2404–2420.

[4] Beladi, H., Farabi, E., Hodgson, P. D., Barnett, M.R., Rohrer, G. S., and Fabijanic, D., 2022, "Microstructure evolution of 316L stainless steel during solid-state additive friction stir deposition," Philosophical Magazine, **102**(7), pp. 618–633.

[5] Perry, M. E. J., Rauch, H. A., Griffiths, R. J., Garcia, D. A., Sietins, J. M., Zhu, Y., Zhu, Y., and Yu, H., 2021, "Tracing plastic deformation path and concurrent grain refinement during additive friction stir deposition," Materialia, **18**, p. 101159.

[6] Chen, G, Wu, K., Wang, Y., Zhu, Z.-X., Nie, P., and Hu, F.-F., 2022, "Effect of rotational speed and feed rate on microstructure and mechanical properties of 6061 aluminum alloy manufactured by additive friction stir deposition," The International Journal of Advanced Manufacturing Technology, **127**(3), pp. 1165–1176.

[7] Martin, P., Luccitti, A., and Walluk, M. R., 2021, "Evaluation of Additive Friction Stir Deposition for the Repair of Cast Al-1.4Si-1.1Cu-1.5Mg-2.1Zn," Journal of Manufacturing Science and Engineering, **144**(6), p. 061006.

[8] Mason, C. J. T., Rodriguez, R. I., Avery, D. Z., Phillips, B. J., Bernarding, B. P., Williams, M.B., Cobbs, S. D., Jordon, J. B., and Allison, P. G., 2021, "Process-structure-property relations for as-deposited solid-state additively manufactured high-strength aluminum alloy," Additive manufacturing, **40**, p. 101879.

[9] Alzahrani, B., El-Sayed Seleman, M. M., Ahmed, M. M. Z., Elfishawy, E., Ahmed, A. M. Z., A., Touileb, K., Jouini, N., and Habba M. I. A., 2021, "The Applicability of Die Cast A356 Alloy to Additive Friction Stir Deposition at Various Feeding Speeds," Materials, **14**(20), p. 6018.

[10] Rahman, M. S., and Chakravarty, U. K., 2021, "Tensile and Fatigue Properties of Ti-6Al-4V Alloy Fabricated by Laser Powder-Bed Fusion Process," Proceedings of the ASME 2020 International Mechanical Engineering Congress and Exposition, Volume 4: Advances in Aerospace Technology, Virtual, Online, November 16–19, 2020, IMECE2020-23672, pp. 1–9.

[11] Rahman, M. S., Pulok, M. K. H., and Chakravarty, U. K., 2022, "Tensile and Fatigue Response of the Laser Powder-Bed Fused Ti-6Al-4V Alloy at High Temperature Conditions," Proceedings of the ASME 2021 International Mechanical Engineering Congress and Exposition, Volume 4: Advances in Aerospace Technology, Virtual, Online, November 1–5, 2021, IMECE2021-72043, pp. 1–8.

[12] Marques, A., Souza, R. A., Pinto, G. A. M., Galdino, A. G. S., and Machado, M. L. P., 2020, "Evaluation of the softening mechanisms of AISI 4340 structural steel using hot torsion Test," Journal of Materials Research and Technology, **9**(5), pp. 10886–10900.

[13] Johnson, G.R. and Cook, W.H., 1985, "Fracture characteristics of three metals subjected to various strains, strain rates, temperatures and pressures," Engineering Fracture Mechanics, **21**(1), pp. 31–48.

[14] Johnson, G.R. and Cook, W.H., 1983, "A Constitutive Model and Data for Metals Subjected to Large Strains, High Strain Rates, and High Temperatures," Proceedings 7th International Symposium on Ballistics, The Hague, April 19-21, 1983, pp. 541–547.

[15] Goanta, V., Munteanu, C., Muftu, S., Istrate, B., Schwartz, P., Boese, S., Ferguson, G., Ciprian, M., and Stefan, A., 2022, "Evaluation of the Fatigue Behavior and Failure Mechanisms of 4340 Steel Coated with WIP-C1 (Ni/CrC) by Cold Spray," Materials, **15**, p. 8116.

[16] Huang, R., and Fukanuma, H., 2015, "6 - Future trends in cold spray techniques," Future Development of Thermal Spray Coatings, pp. 143–162.

[17] Bharathi, K. and Dutta, K., 2016, "Stress Ratio Effect on Ratcheting Behavior of AISI 4340 Steel," IOP Conference Series: Materials Science and Engineering, **115**(1), p. 012016.